Developmental Cell
Article

Angiopoietin-1 Prevents VEGF-Induced Endothelial Permeability by Sequestering Src through mDia

Julie Gavard,[1] Vyomesh Patel,[1] and J. Silvio Gutkind[1,*]
[1]Oral and Pharyngeal Cancer Branch, National Institute of Dental and Craniofacial Research, National Institutes of Health, Department of Health and Human Services, Bethesda, MD 20892-4340, USA
*Correspondence: sg39v@nih.gov
DOI 10.1016/j.devcel.2007.10.019

SUMMARY

Vascular endothelial growth factor (VEGF) and Angiopoietin 1 (Ang1) are both potent proangiogenic factors, but, whereas VEGF causes vascular permeability, Ang1 stabilizes blood vessels and protects them from VEGF-induced plasma leakage. The antivascular permeability mechanisms deployed by Ang1 are still undefined. Here, we demonstrate that Ang1 halts the ability of VEGF to induce the phosphorylation-dependent redistribution of the adhesion molecule VE-cadherin, thereby rescuing the endothelial barrier function. Ang1 inhibits the activation of Src by VEGF, the most upstream component of the pathway linking VEGF receptors to VE-cadherin internalization. Indeed, Ang1 promotes the activation of mDia through RhoA, resulting in the association of mDia with Src. This ultimately deprives VEGF receptors of an essential molecule required for promoting the disruption of endothelial cell-cell contacts and paracellular permeability.

INTRODUCTION

Vascular endothelial growth factor (VEGF) and Angiopoietin 1 (Ang1) play essential and complementary roles in vascular development during embryogenesis. Whereas VEGF is required for the formation of the initial vascular plexus early in development, Ang1 is necessary for the subsequent vascular remodeling into mature blood vessels (Ferrara et al., 1996; Suri et al., 1996). Both VEGF and Ang1 share the ability to promote endothelial survival, proliferation, and migration, by acting on their cognate cell-surface tyrosine-kinase receptors, VEGFR2 (Flk1, KDR) and Tie2 (Tek), respectively (Jones et al., 2001). Aligned with their proangiogenic roles, overexpression of VEGF and Ang1 in the mouse skin results in greatly enhanced tissue vascularity (Suri et al., 1998). However, whereas VEGF causes vascular permeability and tissue edema, Ang1 contributes to the stabilization and the maturation of growing blood vessels (Senger et al., 1983; Thurston et al., 1999). Furthermore, Ang1 administration or overexpression in the dermal compartment can protect from the potentially lethal actions of VEGF as a consequence of uncontrolled plasma leakage (Thurston et al., 2000).

The absence of either Ang1 or Tie2 expression leads to severe defects in blood vessel formation during mouse development characterized by a lack of the periendothelial support (Dumont et al., 1994; Suri et al., 1996). However, Ang1 reduces plasma leakage and strengthens adult vasculature integrity even in the absence of these mural cells (Uemura et al., 2002). In this regard, Ang1 can potently block VEGF-induced endothelial permeability in vitro (Gamble et al., 2000), suggesting that their opposing effects on vascular leakage may be exerted through their direct stimulation of endothelial cells. The molecular mechanisms underlying these clearly distinct, counteracting effects of VEGF and Ang1 on vascular permeability are still undefined. We show here that Ang1 interferes with the ability of VEGF to disrupt the endothelial barrier by preventing Src activation, which is an obligatory component of the pathway by which VEGF provokes vascular permeability (Eliceiri et al., 1999; Gavard and Gutkind, 2006; Weis et al., 2004). At the molecular level, we provide evidence that this process involves the activation of RhoA by Ang1 and the consequent association of mDia, a RhoA downstream target, with Src, thereby preventing the activation of Src by the VEGF receptor VEGFR2. Ultimately, by uncoupling Src to VEGFR2, Ang1 may interfere with the ability of VEGF to initiate the activation of a Src-dependent intracellular signaling route that culminates in the serine phosphorylation-dependent internalization of VE-cadherin and the disassembly of interendothelial adherens junctions, thus preventing VEGF-induced endothelial permeability.

RESULTS

Ang1 Counteracts VEGF-Induced Endothelial Permeability, but Not VEGF Proangiogenic Signaling

As previously described, the subcutaneous administration of VEGF caused dermal vascular permeability accompanied by an increase in VEGFR2 activation (Figure 1A) (Lee et al., 2007; Thurston et al., 2000). Remarkably, coinjection with Ang1 prevented VEGF-induced blood vessel leakiness and plasma leakage, which was assessed by the extravasation of Evans Blue dye in mice (Figures 1B and 1C). To begin investigating the molecular mechanisms underlying the protective effect of Ang1 against VEGF-induced vascular leakage, we first confirmed that Ang1 can directly block the ability of VEGF to induce endothelial permeability in vitro. Indeed, we observed that the pretreatment of endothelial cells with Ang1 for 30 min efficiently prevented the disruption of the endothelial barrier function caused by VEGF, as judged by the passage of FITC-dextran through the endothelial monolayer (Figure 1D). However, both VEGF and Ang1 can promote the proliferation and migration of endothelial cells when used alone or in combination (Figures 1E and 1F). Importantly, the stimulation with

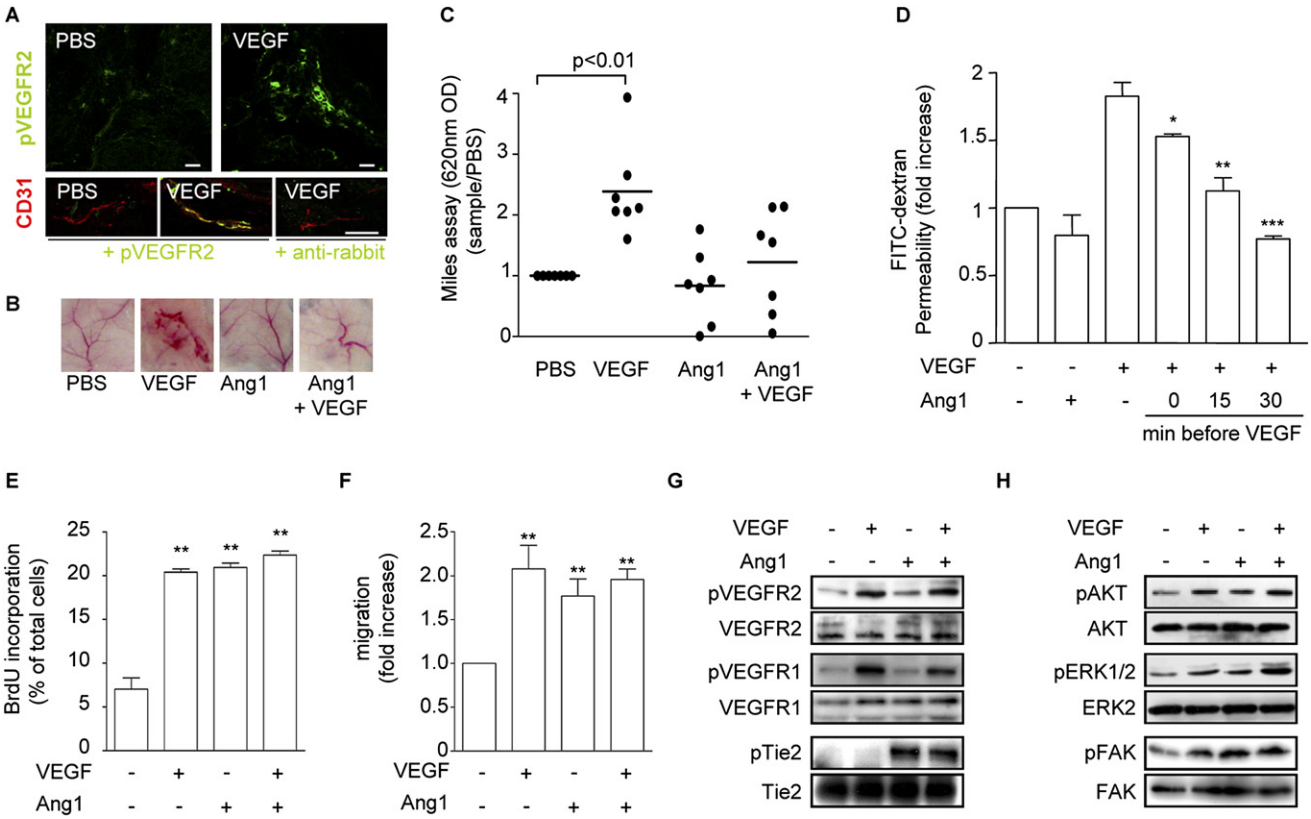

Figure 1. Ang1 Counteracts VEGF-Induced Endothelial Permeability, but Not VEGF Proangiogenic Signaling

(A) Mice were injected subdermally with PBS or with VEGF (50 ng/250 μl) for 1 hr. Tissue sections were stained for pY1054 VEGFR2 (pVEGFR2) and were analyzed by confocal microscopy. Similarly, costaining with CD31 and pVEGFR2 or control antibodies (donkey anti-rabbit) was performed. The scale bars are 10 μm.

(B) Representative pictures of corresponding skin samples after local injection of 250 μl PBS, VEGF (50 ng), Ang1 (50 ng), or a combination of reagents for 1 hr.

(C) The Evans Blue extravasation from the blood vessels was quantified by spectrometry ($OD_{620\ nm}$), n = 7 mice. The median is represented on this scatter plot.

(D) FITC-dextran permeability was determined in overnight-starved, 3-day-old mouse endothelial cell (SVEC) monolayers unstimulated (–) or treated for 30 min with 50 ng/ml VEGF, Ang1, or VEGF after Ang1 treatment (at the indicated times). The data represent FITC-dextran permeability expressed as a fold increase ± SEM with respect to untreated starved cells.

(E) 24 hr-starved endothelial monolayers were left in serum-free (–) media or were stimulated overnight (+, 50 ng/ml) by VEGF and Ang1 alone or in combination. Samples were then incubated with BrdU (10 μM, 4 hr) and were processed for staining and counting. The graph represents the percentage ± SEM of cells showing BrdU-positive nuclei staining.

(F) Endothelial migration was assessed by wound closure of endothelial monolayers treated as described in (E). Data represent the ratio ± SEM between treated and control samples of the distance filled in the wound by endothelial cells.

(G) Overnight-starved, 3-day-old SVEC monolayers (–) were stimulated (+, 50 ng/ml) with VEGF (5 min), Ang1 (30 min), and a combination of the two (Ang1 + VEGF, 25 + 5 min). VEGFR1 and Tie2 tyrosine phosphorylation (p) levels were monitored in VEGFR1 and Tie2 immunoprecipitations, and VEGFR2 activation was assessed by western blots for pY1054 VEGFR2 in total cell lysates. VEGFR1 and two western blots usually show two major bands (200 and 250 kDa).

(H) Cells were processed as described in (G). AKT, ERK, and FAK activation was estimated by using appropriate phosphospecific antibodies, and total AKT, ERK2, and FAK were examined in the same samples.

ANOVA test: ***, $p < 0.001$; **, $p < 0.01$; *, $p < 0.05$.

Ang1, which caused the tyrosine phosphorylation of its receptor, Tie2, did not affect the activation of VEGFR1 and VEGFR2 by VEGF, nor their ability to enhance the phosphorylation of Akt, ERK1/2, and the focal adhesion kinase, three shared downstream signaling events initiated by VEGF and Ang1 (Figures 1G and 1H). Thus, Ang1 can specifically block VEGF-induced permeability, without altering VEGF-initiated proangiogenic signaling.

Ang1 Prevents VEGF-Induced VE-Cadherin S665 Phosphorylation-Dependent Internalization

Recent evidence suggests that VEGF increases endothelial permeability by triggering the destabilization of adherens junctions, a process that involves the removal of adhesive molecules from the surface of endothelial cells (Gavard and Gutkind, 2006; Weis et al., 2004). Notably, VEGF stimulation of endothelial cells labeled with anti-VE-cadherin antibodies results in the rapid accumulation of VE-cadherin-containing intracellular vesicles (Figure 2A). Stimulation with Ang1 not only failed to promote this internalization, but it also halted the accumulation of VE-cadherin in an internal compartment caused by VEGF (Figures 2B and 2C). However, Ang1 did not affect VEGF-induced VEGFR2 internalization (Figure S1; see the Supplemental Data available with this article online) (Lampugnani et al., 2006). Ang1 did not have a general effect on endocytic pathways, as judged by

the effective uptake of transferrin in Ang1-stimulated cells (not shown). However, the tyrosine phosphorylation of VE-cadherin may regulate the endothelial barrier junctions in response to VEGF (Potter et al., 2005). As shown in Figure 2D, VEGF stimulation caused an accumulation of phosphotyrosine-containing VE-cadherin in mature endothelial cell monolayers. Whereas Ang1 did not cause an increase in VE-cadherin tyrosine phosphorylation at early time points (not shown; Gamble et al., 2000), it promoted an increase in phosphotyrosine-containing VE-cadherin after 30 min of stimulation (Figure 2D). However, Ang1 stimulation did not influence the accumulation of phosphotyrosine on VE-cadherin in response to VEGF. This observation prompted us to investigate whether Ang1 alters the phosphorylation of VE-cadherin on its serine 665 residue (S665), which has been recently shown to represent a critical step involved in VE-cadherin trafficking in response to VEGF (Gavard and Gutkind, 2006). The VEGF-induced S665 phosphorylation of VE-cadherin was clearly reduced when cells were pre-exposed to Ang1 (Figure 2D).

To examine the contribution of this particular phosphorylation event to the antagonistic effects of Ang1 on VEGF-induced permeability, we took advantage of the availability of mouse endothelial cells expressing wild-type human (h)VE-cadherin and its phosphomimetic S665D mutant (Gavard and Gutkind, 2006). Similar to endogenous VE-cadherin, Ang1 prevented the internalization of wild-type hVE-cadherin in response to VEGF stimulation. However, Ang1 failed to limit the intracellular accumulation of S665D hVE-cadherin (Figure 2E). Aligned with these observations, Ang1 could not prevent the basal or VEGF-provoked permeability in endothelial cells expressing the phosphomimetic mutant S665D of hVE-cadherin (Figure 2F). Thus, our data suggest that whereas Ang1 can potently block the disruption of the endothelial barrier function caused by VEGF, it cannot prevent the disassembly of endothelial junctions, and hence increased permeability, once VE-cadherin is phosphorylated and targeted for internalization.

Using the acute in vivo vascular permeability model described above, we observed that the morphology of the blood vessels was not altered after VEGF or Ang1 injections, as judged by the wrapping of the endothelial cells (CD31 positive) by the smooth muscle cells (αSMA positive, not shown). However, confocal microscopy analysis of endothelial markers in the skin of control and VEGF-treated mice revealed that vascular permeability was concomitant with the ability of VEGF to trigger VE-cadherin redistribution. VE-cadherin is found primarily on the cell surface along CD31 staining and displays a polarized accumulation into cell junctions in control mice, but VE-cadherin presents a more diffuse, nonpolarized intracellular distribution pattern after VEGF stimulation (Figure 2G). These changes in VE-cadherin localization in response to VEGF exposure are massive (65% of blood vessels), and specific, as VEGF does not affect the distribution of other cell-surface molecules, such as CD31, and are reduced to nearly baseline conditions when VEGF is administered with Ang1 (<25%, Figure 2H). This ability of Ang1 to prevent the VE-cadherin redistribution caused by VEGF in blood vessels is consistent with the potent antagonist effect of Ang1 on VEGF-induced acute vascular permeability. Importantly, aligned with our in vitro observations, protein preparations from dorsal skin of VEGF-treated mice revealed that VEGF promotes the rapid and sustained augmentation of S665 VE-cadherin phosphorylation in vivo, which was prevented by the administration of Ang1 (Figure 2I).

Ang1 Blocks VEGF-Triggered Src Activation

Since VEGF causes VE-cadherin endocytosis through a biochemical route that involves the sequential activation of Src, Vav2, Rac1, and PAK (Gavard and Gutkind, 2006), we tested the specific effects of Ang1 on this signaling axis. Prestimulation with Ang1 prevented the VEGF-initiated activation of Src-family kinases (SFK), Vav2, and Rac (Figures 3A; Figure S2). Similarly, Ang1 decreased the accumulation of phosphorylated PAK in response to VEGF (not shown), together suggesting that Ang1 may interfere with the ability of VEGF to elevate the activity of a Src-initiated pathway that culminates in the serine phosphorylation and internalization of VE-cadherin. Moreover, the use of an active Src mutant circumvented the inhibitory activity of Ang1 on VEGF-induced permeability (Figure S3). We then examined in more detail which specific SFK can be affected by Ang1. Endothelial cells express Src and its related nonreceptor tyrosine kinases Fyn and Yes (Eliceiri et al., 1999), all of which were activated in response to VEGF, as judged by their detection with antibodies recognizing the phosphorylated active state (pSFK) in the corresponding immunoprecipitates (Figure 3B). Among them, however, Src was the only SFK efficiently associated with VEGFR2, in agreement with a prior report (Chou et al., 2002). Using a similar procedure, we found that Ang1 prevented the activation of Src and Fyn, but not Yes (Figure 3C). To challenge the biological significance of these observations, we used histamine, a well-known mediator of vascular permeability. This effect was insensitive to SFK blockade, and was thus likely SFK independent (Figure S4). In addition, Ang1 had only a modest effect on histamine-induced permeability when compared to its remarkable opposition to VEGF, suggesting that Ang1 may be more effective in preventing endothelial permeability when promoted by the activation of SFK-dependent pathways. We next investigated whether Ang1 can impede VEGF-induced SFK activation in vivo. Indeed, SFK phosphorylation was greatly enhanced upon VEGF stimulation, which was prevented when coadministered with Ang1 (Figure 3D). As Src represents the most upstream component of the pathway linking VEGFR2 to endothelial permeability, and both genetic and pharmacological studies indicate that Src activity, but not Fyn, is strictly required for VEGF-induced vascular leakage in vitro and in vivo (Eliceiri et al., 1999; Gavard and Gutkind, 2006), we decided to focus our attention on this nonreceptor tyrosine kinase.

To further investigate how Ang1 affects the dynamic regulation of Src by VEGF, we used a FRET-based Src reporter system (Figure 3E) (Ting et al., 2001). The emission spectra of control experiments indicated that, when the CFP donor is excited at 433 nm, an energy transfer occurred at the YFP peak (527 nm) only in VEGF-stimulated cells (Figure 3F). Remarkably, this VEGF-dependent FRET was abolished by Ang1 as well as by a SFK inhibitor (su6656). More importantly, this approach revealed that the time course of VEGF stimulation is consistent with a two-step activation of Src, which is sustained for at least 30 min (Figure 3G), and that Ang1 can reduce these two peaks of VEGF-initiated Src activation. Quantitative analysis of single-cell image-based FRET assays also indicated that Src is activated in more than 80% of the endothelial cells (not shown), with a high

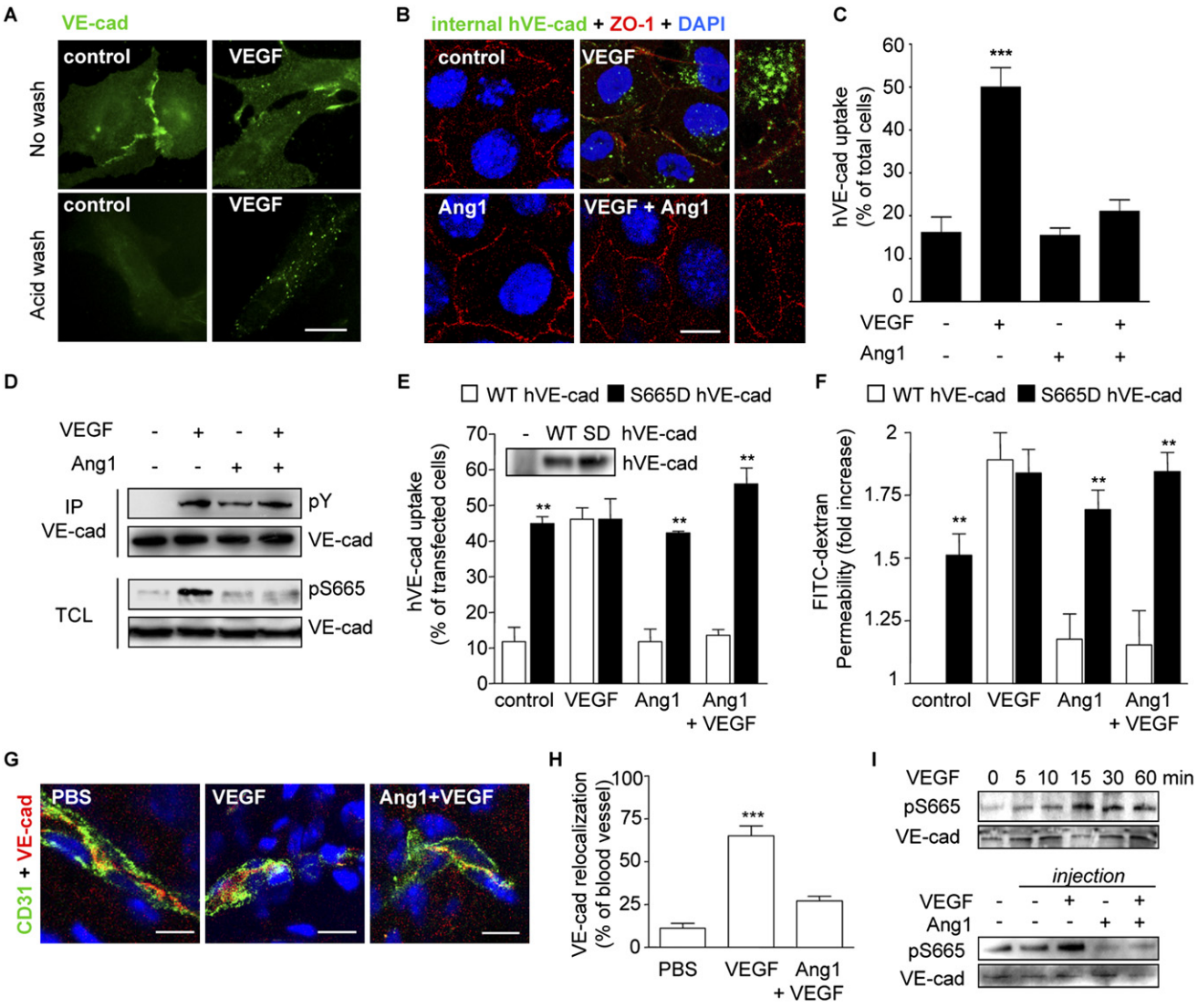

Figure 2. Ang1 Prevents VEGF-Induced VE-Cadherin S665 Phosphorylation-Dependent Internalization

(A) Human endothelial cells were incubated with anti-human VE-cadherin antibody at 4°C to label cell-surface-exposed VE-cadherin and were then placed at 37°C for 30 min to track its movements, in serum-free medium (control) or with VEGF (50 ng/ml). Cells were fixed ("no wash") or subjected to mild acid wash ("acid wash") before fixation in order to remove membrane-bound antibodies. This treatment reveals acid-resistant internal anti-VE-cadherin antibodies. The scale bar is 10 μm.

(B) Cells were treated as indicated in (A) in serum-free medium (control) with 50 ng/ml VEGF, Ang1, and VEGF after Ang1 treatment. Cells were further stained for ZO-1 (red). Only the internal VE-cadherin (green) is resistant to the acid-wash treatment while the cell-surface staining is removed. The scale bar is 10 μm.

(C) Quantification of the number of cells exhibiting vesicle staining in the VE-cadherin-uptake experiments and expressed as the mean percentage of total cells ± SEM. Cells were stimulated as indicated in (B), $n > 300$.

(D) Overnight-starved, 3-day-old SVEC monolayers (–) were stimulated (+, 50 ng/ml) by VEGF (5 min), Ang1 (30 min), and a combination of the two (Ang1 + VEGF, 25 + 5 min). Cell lysates were analyzed for phosphotyrosine (pY), via western blot, in the VE-cadherin (VE-cad) immunoprecipitates (IPs). Total cell lysates were analyzed for phosphoS665-VE-cadherin (pS665) and total VE-cadherin (VE-cad) contents.

(E) Quantification of the number of cells exhibiting vesicle staining in the VE-cadherin-uptake experiments and expressed as the mean percentage of transfected cells ± SEM in mouse SVECs expressing WT (white bar) and S665D (black bar) human (h)VE-cadherin. Cells were stimulated as indicated in (B), $n > 300$. The level of expression of the human WT VE-cadherin and SD is shown in transfected mouse SVECs, by using the BV6 human-specific anti-VE-cadherin antibody.

(F) FITC-dextran permeability was determined in overnight-starved, 3-day-old SVEC monolayers, transfected with WT (white bar) and S665D (black bar) hVE-cadherin, and treated as described in (B). The data represent FITC-dextran permeability expressed as fold increase ± SEM with respect to untreated, starved cells.

(G) Representative confocal acquisitions of CD31 (green) together with VE-cadherin (red) performed on ethanol-fixed, frozen 3 μm sections from skin samples injected with 250 μl saline (–), VEGF (50 ng), or Ang1 + VEGF (50 ng of each) after 1 hr. The scale bars are 20 μm.

(H) VE-cadherin redistribution was quantified based on z-stack reconstructions in frozen sections from five different animals. A positive score was attributed when VE-cadherin and CD31 staining were not colocalized. The graph represents the percentage ± SEM of blood vessels exhibiting this delocalized VE-cadherin pattern per random field.

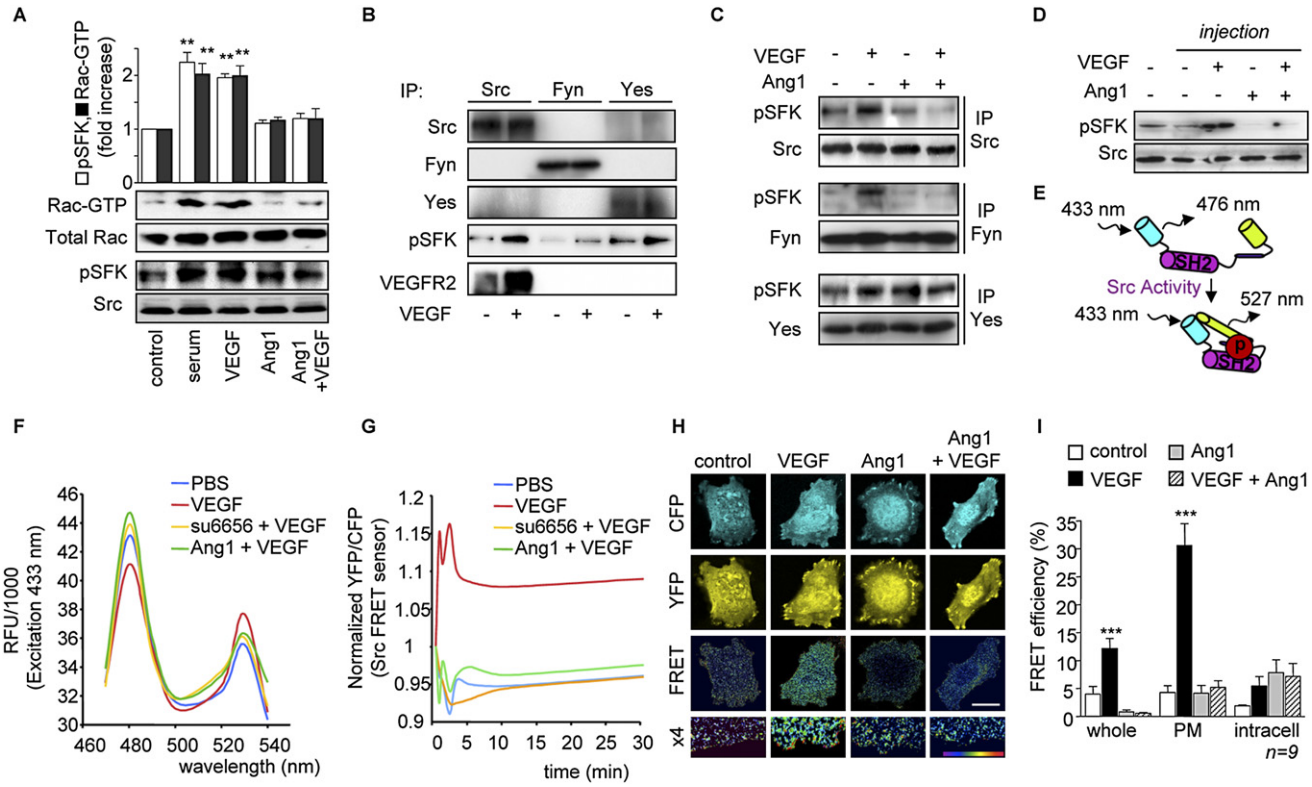

Figure 3. Ang1 Blocks VEGF-Triggered Src Activation

(A) Overnight-starved, 3-day-old SVEC monolayers (control) were stimulated by 10% serum as a positive control, VEGF (50 ng/ml, 5 min), Ang1 (50 ng/ml, 30 min), and a combination of the two (Ang1 + VEGF, 25 + 5 min). The Rac activation was assessed by GST-CRIB pull-down (Rac-GTP), and Src activation was assessed by anti-phosphoY418-SFK antibodies (pSFK) in total cell lysates. Total levels of Rac and Src were also evaluated in the same samples. The graph shows the relative pixel intensity, measured by the NIH Image J software. Bar graphs show the average ± SEM.

(B) Similarly, cells were treated with VEGF (+) and processed for Src, Fyn, and Yes immunoprecipitations (IPs). IPs were then processed for western blots against Src, Fyn, Yes, pSFK, and VEGFR2.

(C) Cells were treated as described in (A), and protein extracts were subjected to Src, Fyn, or Yes IPs. Western blots for pSFK were then performed in each IP.

(D) Proteins were extracted from mouse skins that were either noninjected or were injected with 250 μl saline (−), VEGF (50 ng), Ang1 (50 ng), or a combination of the two for 1 hr, and they were analyzed by western blot against phosphoY418-SFK (pSFK) and total Src.

(E) Schematic representations of the Src FRET biosensor in the case of quiescent and energy transfer conformations, dependent on the Src activity status. Once activated, Src may phosphorylate its substrate (P), which showed higher affinity for the SH2 domain, bringing YFP closer enough to CFP for energy transfer.

(F) Wavelength emission spectra between 470 and 540 nm, measured each 20 nm, when excited at 433 nm. The CFP peak (donor) is around 480 nm, and the YFP peak (acceptor) is around 530 nm. Cells were either nonstimulated (PBS) or were stimulated by VEGF (50 ng/ml, 5 min) and after su6656 (SFK inhibitor, 1 μM, 30 min) and Ang1 (50 ng/ml, 30 min) treatments. Curves represent the average ratio from three independent experiments, each done in triplicate.

(G) FRET is represented as the normalized YFP/CFP ratio (527/476 nm emission fluorescence, when excited at 433 nm). Cells were stimulated as described in (F) for the indicated period of times. Curves represent the average ratio from three independent experiments, each done in triplicate.

(H) FRET efficiency was monitored in SVECs that were unstimulated (control) or were stimulated by 50 ng/ml VEGF (5 min), Ang1 (25 min), or a combination of the two (Ang1 + VEGF, 25 + 5 min). Energy transfer is color-coded (from purple to red). The scale bar is 20 μm.

(I) Quantification of FRET efficiency calculated by the Youlan method either in the total cell area (whole), at the plasma membrane area (PM), or in the intracellular part, excluding the cell border (intracell), n = 9 cells. Bar graphs show the average ± SEM.

ANOVA test: ***, $p < 0.001$; **, $p < 0.01$.

FRET efficiency (15%) after a 5 min stimulation (Figures 3H and 3I). Aligned with the data obtained by using spectral FRET of whole-cell populations, this single-cell Src activation-based FRET analysis showed that VEGF stimulation of Src was strongly blocked by Ang1 pretreatment (Figures 3H and 3I). We also noticed that this effect was even more pronounced when analyzing the status of Src activation at the level of the plasma membrane (Figure 3I). Taken together, these observations suggested that Ang1 may interfere with VEGF-induced endothelial barrier destabilization by preventing Src activation, which is an obligatory component of the pathway by which VEGF provokes vascular permeability.

(I) Western blot analysis was performed for phosphoS665-VE-cadherin (pS665) and VE-cadherin (VE-cad) from mice injected with saline (−) or VEGF (50 ng/250 μl) at the indicated times. Alternatively, proteins were extracted from mouse skins that were either noninjected or were injected with 250 μl saline (−), VEGF (50 ng), Ang1 (50 ng), or a combination of the two for 1 hr.

ANOVA test: ***, $p < 0.001$; **, $p < 0.01$; *, $p < 0.05$.

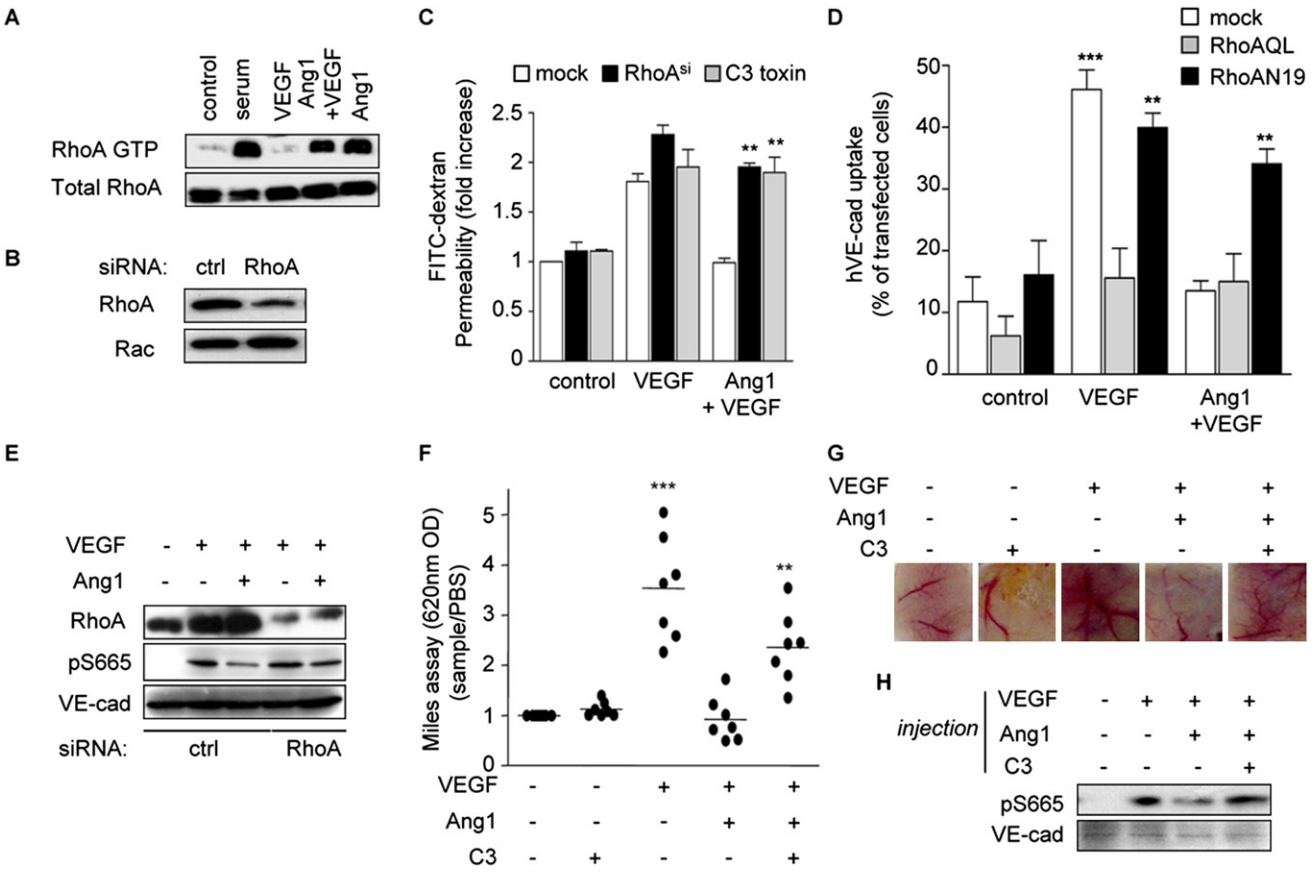

Figure 4. Activation of RhoA by Ang1 Protects from VEGF-Induced Permeability

(A) Overnight-starved, 3-day-old SVEC monolayers (control) were stimulated by 10% serum as a positive control, VEGF (50 ng/ml, 5 min), Ang1 (50 ng/ml, 30 min), and a combination of the two (Ang1 + VEGF, 25 + 5 min). RhoA activation (RhoA-GTP) was assessed by GST-rhotekin pull-down. RhoA was used as a loading control in total cell lysates.

(B) SVECs were transfected with nonsilencing (ctrl, 50 nM) or RhoA (50 nM) duplexes. RhoA protein levels were assessed 3 days later; Rac was used as a loading and specificity control in the same samples.

(C) FITC-dextran permeability was determined in starved, 3-day-old SVEC monolayers transfected by mock DNA (white bar), RhoA siRNA (50 nM, black bar), and C3 toxin (gray bar). Cells were nonstimulated (control) or were treated for 30 min with 50 ng/ml VEGF alone or after Ang1 treatment. Bar graphs show the average ± SEM.

(D) Quantification of the number of cells exhibiting VE-cadherin vesicle staining in the uptake experiments either in serum-free media (control) or when incubated for 30 min with 50 ng/ml VEGF alone or after Ang1 treatment; quantification was expressed as the mean percentage of transfected cells ± SEM in SVECs expressing GFP (mock, white bar), active RhoAQL (gray bar), and inactive RhoAN19 (black bar).

(E) SVECs were transfected with nonsilencing (ctrl) or RhoA duplexes (50 nM). Two days later, starved-overnight SVEC monolayers (−) were stimulated by VEGF (50 ng/ml, 5 min) alone or after Ang1 stimulation (Ang1 + VEGF, 25 + 5 min). PhosphoS665-VE-cadherin (pS665), RhoA, and VE-cadherin protein levels were monitored in the same samples.

(F) Mice were injected with 250 μl PBS, VEGF (50 ng), Ang1 (50 ng), and C3 toxin plus tetanolysin (1 μg). The extravasation of Evans Blue from the blood vessels was quantified by spectrometry ($OD_{620\ nm}$), n = 7 mice. The median is represented on this scatter plot.

(G) Representative pictures of corresponding skin samples treated as described in (F).

(H) Protein extracts from skin were prepared as described above, and phosphoS665-VE-cadherin (pS665) and VE-cadherin (VE-cad) protein levels were monitored in the same samples.

ANOVA test: ***, $p < 0.001$; **, $p < 0.01$.

Activation of RhoA by Ang1 Protects from VEGF-Induced Permeability

In search for a likely mechanism by which Ang1 could prevent SFK activation by VEGF, we focused on the fact that Ang1 blocks the VEGF-dependent activation of Rac1 without interfering with other components of the VEGFR signaling axis. As small GTP-binding proteins often regulate the activity of each other (Burridge, 1999), we asked whether this proangiogenic factor stimulates a distinct member of the Rho-family GTPases. First, we observed that Ang1 can transiently activate Rho in the endothelial monolayer (Figure 4A), as earlier reported (Cascone et al., 2003). Interestingly, the ability of VEGF to cause endothelial permeability in the presence of Ang1 was restored when RhoA expression was decreased by siRNA or its activity was blocked by the use of the C3 toxin, supporting a role for RhoA signaling in the antipermeability pathway deployed by Ang1 in the presence of VEGF (Figures 4B and 4C). VE-cadherin endocytosis was also affected by RhoA activation, as expression of the

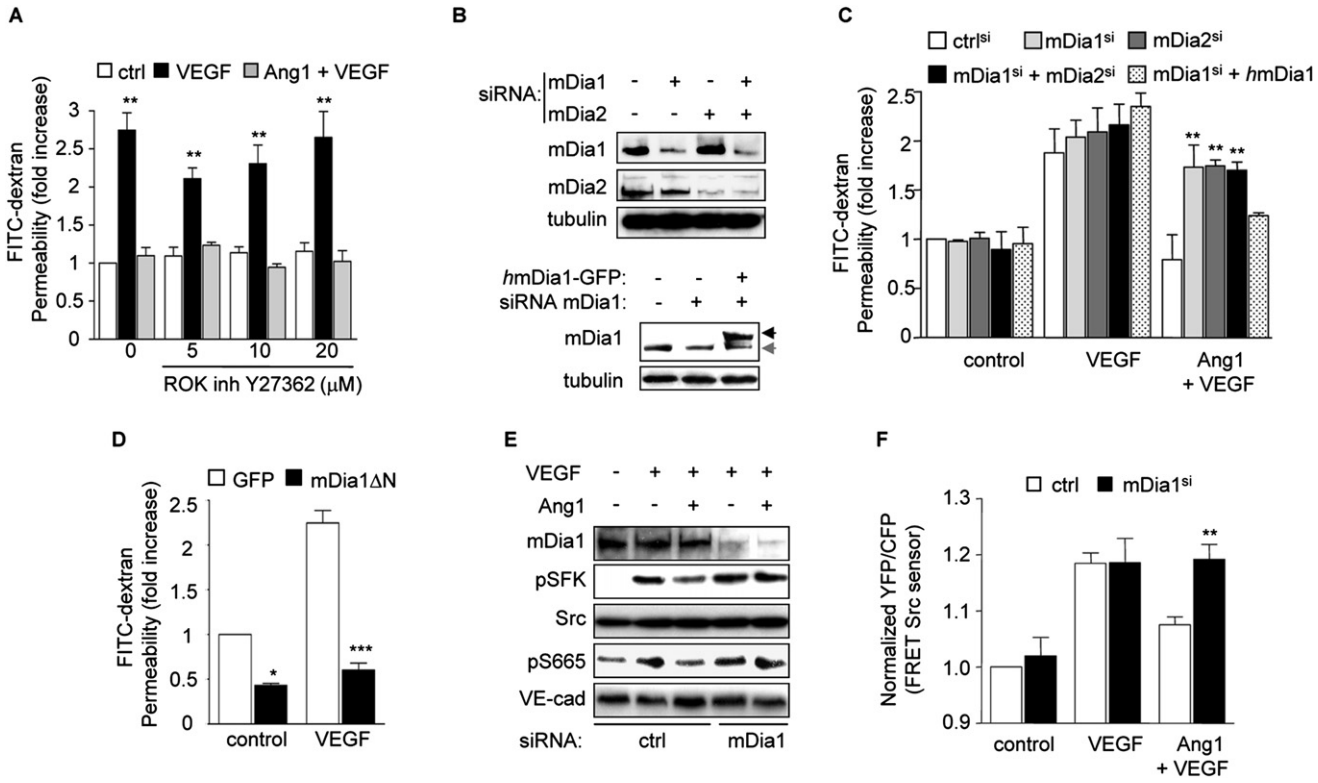

Figure 5. mDia Is Required Downstream of Ang1 to Block VEGF-Dependent Permeability

(A) FITC-dextran permeability was determined in 3-day-old, starved SVECs (control, white bar), stimulated 30 min by 50 ng/ml VEGF alone (black bar) and after Ang1 stimulation (gray bar). Cells were treated with increasing amounts of Y27632 ROK inhibitor (5, 10, and 20 μM). Bar graphs show the average ± SEM.

(B) SVECs were transfected with 50 nM nonsilencing (–), mDia1, and mDia2 duplexes, alone or together. mDia1 and mDia2 protein levels were assessed 3 days later. Alternatively, SVECs treated for 2 days with 50 nM nonsilencing (–) or mDia1 duplexes were transfected with GFP (–) or human (*h*) mDia1-GFP and were further analyzed by western blot 1 day later. Endogenous mDia1 is indicated by a gray arrow; exogenous mDia1-GFP is indicated by a black arrow. Tubulin was used as a loading control.

(C) FITC-dextran permeability was determined in 3-day-old, starved SVEC monolayers transfected by control duplexes (ctrl^{si}, white bar), mDia1 siRNA (light-gray bar, ^{si}), and mDia2 siRNA (dark-gray bar, ^{si}), both mDia1 and mDia2 (50 nM of each, black bar), or in mDia1 siRNA + *h*mDia1-GFP (dashed bar). Cells were non-stimulated (control) or were treated for 30 min with 50 ng/ml VEGF alone or after Ang1 stimulation. Bar graphs show the average ± SEM.

(D) FITC-dextran permeability was determined in 3-day-old GFP- (white bar) and mDia1-ΔN- (black bar) transfected, starved SVECs that were stimulated by VEGF (50 ng/ml, 30 min). Bar graphs show the average ± SEM.

(E) SVECs were transfected with nonsilencing (ctrl) or mDia1 duplexes (50 nM). Three days later, overnight-starved SVEC monolayers (–) were stimulated by 50 ng/ml VEGF alone (5 min) and after Ang1 stimulation (25 + 5 min). mDia1, SFK activation (pSFK), Src, phosphoS665-VE-cadherin (pS665), and VE-cadherin protein levels were monitored in the same samples.

(F) SVECs were transfected with nonsilencing (ctrl, white bar) or mDia1 duplexes (50 nM, black bar), and were transfected 2 days later with the Src FRET sensor. FRET efficiency as the normalized YFP/CFP ratio was then measured in unstimulated cells (control) or in cells stimulated by 50 ng/ml VEGF alone (5 min) and after Ang1 stimulation (25 + 5 min). Bar graphs show the average ± SEM.

ANOVA test: ***, $p < 0.001$; **, $p < 0.01$; *, $p < 0.05$.

dominant-negative RhoA mutant enabled the VE-cadherin uptake induced by VEGF to occur even in the presence of Ang1 (Figure 4D). In agreement, the knockdown of endothelial RhoA by siRNA restored the VEGF-induced S665 VE-cadherin phosphorylation that was blocked by Ang1 (Figure 4E). We next utilized the local treatment with C3 toxin to investigate the contribution of RhoA to the anti-VEGF permeability effect of Ang1 in vivo. We did not observe any short-term effects of C3 toxin injection, alone or with VEGF, on blood vessel morphology and skin histology (not shown). However, C3 toxin was sufficient to prevent the antipermeability effect of Ang1 and therefore restored the VEGF-induced S665 VE-cadherin phosphorylation and vascular leakage (Figures 4F–4H). This supported the emerging notion that Ang1 utilizes RhoA-initiated signaling pathways to offer protection from the disruption of the endothelial barrier caused by VEGF.

mDia Is Required Downstream of Ang1 to Block VEGF-Dependent Permeability

Based on these results, we explored whether ROK, a key downstream target for Rho, could participate in the signaling route by which Ang1 interferes with VEGF-induced permeability. However, pharmacological inhibition of ROK did not affect the blocking effect of Ang1 (Figure 5A). The efficiency of this drug was confirmed by virtue of its ability to inhibit myosin-light chain phosphorylation (not shown). In search for alternative Ang1/RhoA pathways impinging on Src, we next investigated the potential role of mDia, another typical RhoA target (Wallar and

Alberts, 2003). We first observed that Ang1 stimulation enhances the formation of a heterocomplex between mDia1 and mDia2, which was confirmed by knocking down each of these mDia proteins (Figure S5). Interestingly, knocking down either mDia1 or mDia2 eliminated the counteracting effect of Ang1 on VEGF-induced endothelial permeability in mouse endothelial cells, which was rescued by the expression of a human mDia1-GFP fusion protein (Figures 5B and 5C). No additional effect of knocking down both mDia1 and mDia2 was observed (Figure 5C), suggesting that the availability of both proteins is limiting, and that mDia1 and mDia2 activities are functionally linked, in agreement with their ability to form a homo- and heterocomplex (Copeland et al., 2007).

Supporting that, once activated, mDia plays a key role for Ang1 in controlling endothelial barrier function, the expression of an active mDia1 mutant was sufficient to block VEGF-induced permeability (Figure 5D). Both western blot and FRET analysis showed that reducing the expression of mDia1 did not affect basal or VEGF-stimulated levels of active Src, but restored the ability of VEGF to activate SFK signaling and to promote the accumulation of VE-cadherin phosphorylated on S665 when cells were exposed to Ang1 (Figures 5E and 5F). Thus, these observations suggest that mDia acts downstream of RhoA in the biochemical route by which Ang1 counteracts the VEGF-initiated permeability signaling pathway.

A Pool of Src Is Sequestered by mDia upon Ang1 Stimulation

Of interest, these findings may explain the requirement of p190RhoGAP for Ang1 signaling (Mammoto et al., 2007), as the hydrolysis of GTP bound to RhoA may be necessary for the subsequent dissociation of active mDia from RhoA. How does mDia, in turn, play a role in the blocking effect of Ang1 on the VEGF-increased permeability? One possibility is that activated mDia strengthens the endothelial cell barrier function by stabilizing microtubules (Birukova et al., 2005; Palazzo et al., 2001). However, the observation that mDia can directly interact with Src through its Src homology (SH)3 domain (Tominaga et al., 2000) prompted us to ask whether mDia1 could affect the activation of Src by VEGF or its inhibition by Ang1. Ang1, but not VEGF, stimulation caused an increased association of mDia1 with Src, in a slow but sustained fashion (Figure 6A; Figure S6). This was also true for Fyn and Yes, which associated with mDia1 in response to Ang1 (Figure 6B). Mammalian or recombinant Src interacted with mDia1, only in its open conformation, as judged by the use of mDia1 N-terminal deletion mutants or by favoring its active state by a brief heat shock (Figure 6C; Figure S5). Finally, Src activity may not be required for this interaction, as inhibition of Src activation with a SFK blocker did not interfere with the Src/mDia1 association caused by Ang1 (Figure 6D). In contrast, the knockdown of endogenous RhoA abolished the Ang1-induced Src/mDia interaction, together indicating that the activation of mDia1 through RhoA is necessary to promote the formation of stable Src/mDia complexes in response to Ang1 (Figure 6E).

As shown in Figure 2, VEGF induces the binding of VEGFR2 to Src. However, the treatment with Ang1 prevented the accumulation of VEGFR2/Src complexes upon VEGF stimulation (Figure 6F). Concomitant with this decrease, Ang1 promoted the increased association of Src and mDia1 in a VEGFR2-free pool, as suggested by VEGFR2 immunodepletion experiments (Figure 6G). In fact, mDia1 can compete for binding to Src with VEGF-stimulated VEGFR2, as judged by the decreased formation of VEGFR2/Src complexes upon increased expression levels of active mDia1 in endothelial cells (Figure 6H). This suggests that the interaction of Src with mDia1 and VEGFR2 are mutually exclusive, and therefore that mDia1 may limit the pool of Src available for interaction with VEGFR2. Remarkably, the inhibitory effect of Ang1 on VEGFR2/Src complex formation was reverted by decreasing the expression levels of RhoA and mDia1 (Figure 6I). Together, these findings support the emerging notion that, in endothelial cells, the activation of RhoA by Ang1 results in the interaction of mDia1 with Src, thereby preventing the binding of Src to VEGFR2 and the consequent activation of a SFK-dependent pathway that involves Vav2, Rac1, and PAK that leads to the phosphorylation and internalization of VE-cadherin, and ultimately to the disassembly of cell-cell junctions and enhanced vascular permeability (Figure 7). Thus, by limiting the access of Src to VEGFR2, mDia1 may restrict the activation of the SFK-initiated pathway and ultimately orchestrate the interplay between Ang1 and VEGF, and its biological outcome.

DISCUSSION

VEGF and Ang1 play essential roles in vascular development and in adult blood vessel function (Dumont et al., 1994; Ferrara et al., 1996; Lee et al., 2007; Suri et al., 1996). Whereas both act as proangiogenic factors, VEGF and Ang1 elicit strikingly distinct responses regarding vascular permeability and plasma leakage (Thurston et al., 1999, 2000). Here, we provide evidence of a novel, to our knowledge, molecular mechanism by which Ang1 specifically counteracts VEGF-induced permeability. Our data indicate that Ang1 activation of its cognate receptor, Tie2, triggers the activation of RhoA, which, in turn, leads to the stimulation of one of its downstream targets, mDia. Activated mDia binds Src, thereby inhibiting the activation of this nonreceptor tyrosine kinase by the VEGF receptor. By causing the sequestration of Src, the Ang1 signaling pathway may ultimately deprive VEGFR2 of an essential molecule required to initiate a signaling route that includes Vav2, Rac1, and PAK, and culminates in the phosphodependent internalization of VE-cadherin, thus causing the disassembly of interendothelial junctions and enhancing endothelial permeability (Garrett et al., 2007; Gavard and Gutkind, 2006; Stockton et al., 2004; Weis et al., 2004).

Ang1 might exert a general antivascular permeability effect, protecting blood vessels from the plasma leakage caused by VEGF, as well as by thrombin and bacterial wall components, such as LPS (Li et al., 2004; Mammoto et al., 2007). In contrast to Ang1, which stimulates RhoA and mDia, thrombin and LPS enhance vascular permeability through a robust and persistent RhoA activation and the consequent ROK-dependent assembly of stress fibers and cell contraction (Wojciak-Stothard and Ridley, 2002). The strength and location of RhoA activation may therefore affect the choice of the RhoA downstream target, thereby determining whether RhoA-initiated signals protect the barrier function of endothelial cells or promote vascular leakage. In addition, Ang1 acts as a vascular protective factor by limiting leukocyte and neutrophil adhesion and transmigration through

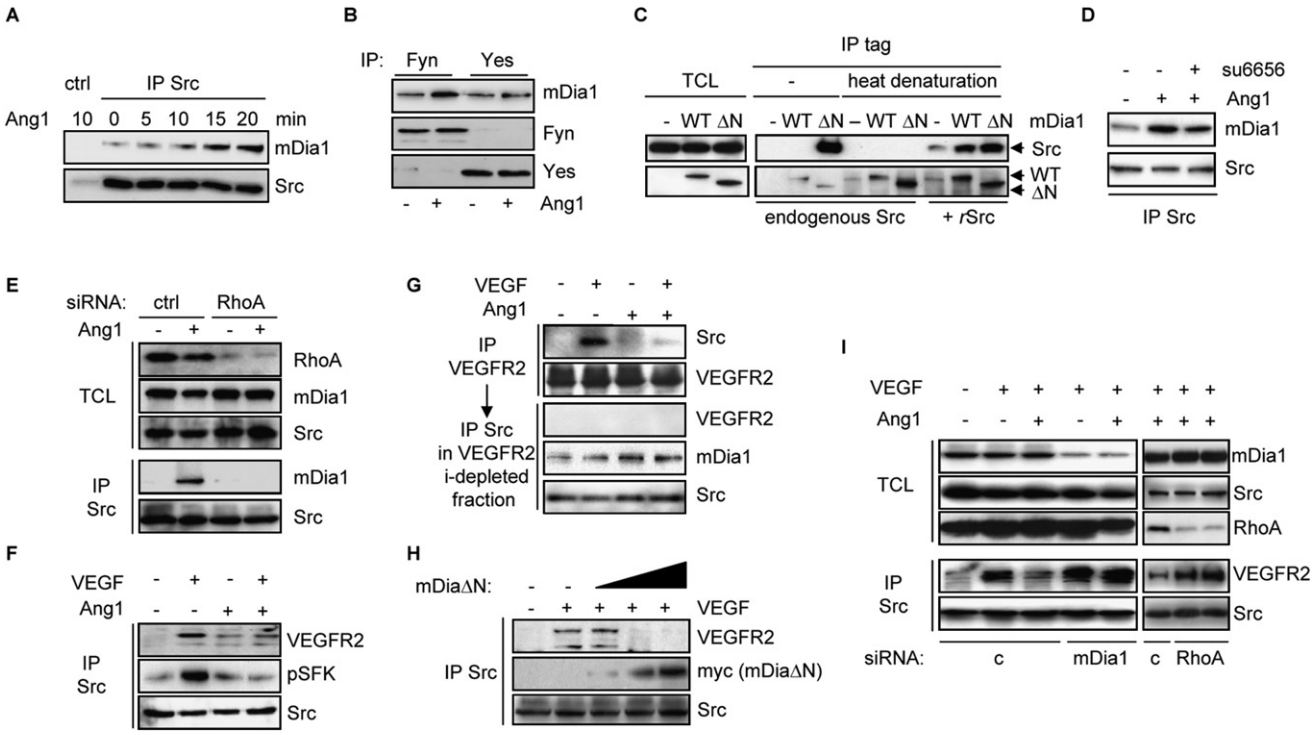

Figure 6. A Pool of Src Is Sequestered by mDia upon Ang1 Stimulation

(A) Overnight-starved, 3-day-old SVEC monolayers were stimulated by Ang1 (50 ng/ml, from 0 to 20 min) and subjected to Ig control (ctrl) or Src immunoprecipitation (IP). mDia1 and Src protein levels were evaluated in the IP fractions.

(B) Overnight-starved, 3-day-old endothelial monolayers were stimulated by Ang1 (50 ng/ml, 15 min) and subjected to Fyn or Yes IP. mDia1, Fyn, and Yes protein levels were evaluated in the IP.

(C) HEK293T cells were transfected with GFP (–), GFP-mDia wild-type (WT), and myc-active mDia (ΔN) and were lysed for tag IP (GFP or myc). IPs were collected or further subjected to heat shock (99°C, 2 min), washed, and subsequently incubated with 2 μg recombinant Src (*r*Src). Src, GFP (WT), and myc (ΔN) western blots were then performed in total cell lysates or IPs.

(D) Overnight-starved, 3-day-old SVEC monolayers were stimulated by Ang1 (50 ng/ml, 15 min) alone and after stimulation with SFK inhibitor (su6656, 1 μM, 30 min). mDia1 and Src protein levels were evaluated in the Src IP.

(E) SVECs were transfected with nonsilencing (ctrl) or RhoA duplexes (50 nM, 3 days). Overnight-starved SVECs (–) were stimulated by Ang1 (50 ng/ml, 15 min) and were analyzed for RhoA, mDia1, and Src protein levels in the total cell lysate. mDia1 and Src were also analyzed in the Src IP.

(F) Overnight-starved SVECs (–) were stimulated (+, 50 ng/ml) by VEGF (5 min), Ang1 (30 min), and a combination of the two (25 + 5 min). VEGFR2 levels, pSFK, and Src were monitored in the Src IP.

(G) Overnight-starved SVECs (–) were stimulated as described in (F). Src and VEGFR2 levels were monitored in VEGFR2 IPs. The output from this VEGFR2 IP (VEGFR2 i-depleted fraction) was then cleared from VEGFR2 antibodies by incubation with G protein Sepharose and was subjected to Src IP. Levels of VEGFR2, mDia1, and Src were then evaluated.

(H) SVECs were transfected with mock (–) or an increased amount of myc-active mDia1 (ΔNmDia1: 1, 3, and 5 μg). Overnight-starved, 3-day-old SVEC monolayers were stimulated by VEGF (50 ng/ml, 5 min), and protein extracts were subjected to Src IP. Levels of VEGFR2, ΔNmDia1 (myc), and Src were then evaluated.

(I) SVECs were transfected with nonsilencing (c), mDia1, or RhoA duplexes (50 nM). Three days later, overnight-starved SVECs (–) were stimulated for 5 min with 50 ng/ml VEGF alone or after Ang1 stimulation (25 min). VEGFR2 and Src protein levels were monitored in the Src IP. mDia1, Src, and RhoA were also evaluated in the total cell lysate.

the endothelial barrier (Gamble et al., 2000; Pizurki et al., 2003). Thus, the Ang1/Tie2 endothelial signaling axis might play a key anti-inflammatory role in various diseases such as asthma, rheumatoid conditions, and septic shock. Whether Ang1 also acts by preventing Src activation in each of these cases, alone or in combination with other potential mechanisms, such as by affecting the activation of PKC, calcium signaling, or GAPs for RhoGTPases (Jho et al., 2005; Li et al., 2004; Mammoto et al., 2007), is at the present unknown and warrants further investigation. In this regard, the complete delineation of the specific molecular mechanisms by which each class of vascular leakage factors acts may facilitate the identification of additional targets for the antipermeability action of Ang1.

However, the discovery that Ang1 is a proangiogenic factor but blocks rather than promotes vessel leakiness has opened the possibility of using Ang1 for therapeutic purposes in many pathological conditions characterized by enhanced vascular leakiness, such as in acute and chronic inflammation, diabetic retinopathy, macular degeneration, and tumor-induced angiogenesis. One can anticipate the use of Ang1 together with VEGF to stimulate revascularization of damaged or ischemic tissues while preventing vascular leakage. In this scenario, our present observation that Ang1 rescues the barrier function of the endothelium from VEGF-induced endothelial permeability by stimulating mDia and uncoupling Src from VEGFR2 has now helped define the underlying mechanisms of their counteracting effects. These

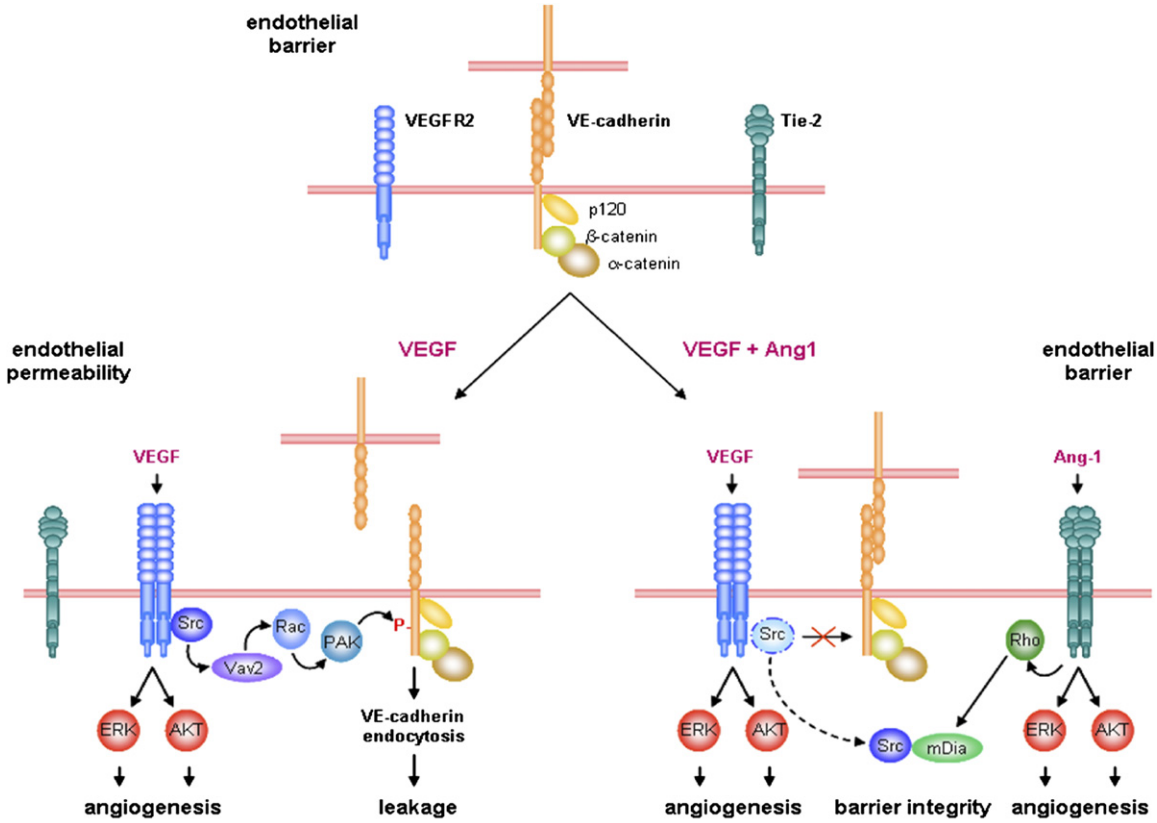

Figure 7. Model Depicting How VEGF and Ang1 Can Both Elicit a Proangiogenic Response, but Control the Endothelial Barrier Function in an Antagonist Fashion
See text for details.

findings may provide a molecular framework for the future exploration of natural and synthetic small molecules that may act on the mDia/Src signaling axis as potential antivascular leakage therapeutic agents.

EXPERIMENTAL PROCEDURES

Cell Culture, Transfections, and siRNA

Immortalized human endothelial cells were obtained from C.J. Edgell (Edgell et al., 1983), and SV40 immortalized mouse endothelial cells (SVECs) and HEK293T cells were purchased from the ATCC (Manassas, VA). DNA transfections were performed by using the Amaxa's electroporation system, achieving ~80% efficiency (Amaxa Biosystems, Gaithersburg, MD). siRNA were delivered with the Hiperfect reagent (QIAGEN, Valencia, CA). The following predesigned sequences were used: nonsilencing sequence (Dharmacon, Chicago, IL) and mouse mDia1, mDia2, and RhoA sequences (Stealth RNAi, Invitrogen, Carlsbad, CA).

Reagents and Antibodies

Recombinant Vascular Endothelial Growth Factor 165 was purchased from Calbiochem (San Diego, CA), Angiopoietin 1 was purchased from R&D Systems (Concord, MA), SFK inhibitor su6656 was purchased from Calbiochem, and C botulinum exoenzyme C3 and tetanolysin were purchased from List Biological Labs (Campbell, CA). The following antibodies were used: mouse anti-human VE-cadherin (BV6 clone, Research Diagnostics, Inc., Flanders, NJ); mouse anti-Rac (BD Biosciences, San Jose, CA); mouse anti-phosphotyrosine (4G10 clone, Upstate Biotech, Waltham, MA); mouse anti-Src (L4A1 clone, Cell Signaling, Boston, MA); mouse anti-tubulin and Yes (Santa Cruz Biotechnology, Santa Cruz, CA); mouse anti-myc (Covance, Berkley, CA); rat anti-CD31 (BD); mouse anti-cadherin (Sigma); rabbit anti-phosphoS473 AKT and phosphoT202/Y204 ERK1/2 (Cell Signaling); rabbit anti-RhoA, VEGFR2, VEGFR1, FAK, Fyn, Tie2, ERK2, and Src (Santa Cruz Biotechnology); rabbit anti-phosphoY418 Src, phosphoY1054 VEGFR2, and phosphoY397 FAK (Biosource QCB, Camarillo, CA); goat anti-VE-cadherin, mDia1, and mDia2 (Santa Cruz Biotechnology). Rabbit anti-phosphoS665 VE-cadherin was described previously (Gavard and Gutkind, 2006). Secondary antibodies for immunofluorescence and western blot were purchased from Jackson ImmunoResearch (West Grove, PA) and Southern Biotechnology (Birmimgham, AL), respectively.

DNA and Constructs

pCEFL-human VE-cadherin wild-type and S665D mutant were described previously (Gavard and Gutkind, 2006), as were pCEFL-AU5-RhoAN19, pCEFL-AU5-RhoAQL, pcDNA3-C3toxin (Marinissen et al., 2004), the N-terminal deletion active mutant pEF-myc-ΔGBDmDia1 (Tominaga et al., 2000), and pEGFP-mDia1 (Seth et al., 2006). The FRET-based Src sensor was provided by R.Y. Tsien (Ting et al., 2001) and was subcloned in pCEFL.

Statistical Analysis

In all cases, results are shown as a mean value ± SEM from at least three independent experiments; confocal pictures and western blot scans are representative of at least three independent experiments. Statistical analysis was performed with Prism 4.2 software (GraphPad). ANOVA test: ***, $p < 0.001$; **, $p < 0.01$; *, $p < 0.05$.

Miles Permeability Assays

All animal studies were carried out according to National Institutes of Health-approved protocols, in compliance with the Guide for the Care and Use of Laboratory Animals. Miles permeability assays were conducted in athymic nude mice (Harlan Sprague-Dawley, Frederick, MD) as described previously (Eliceiri

et al., 1999). Briefly, reagents were injected subdermally in PBS as a maximal volume of 250 μl, and the injection zone was marked for further analysis. Sterile Evans Blue dye (150 μl, 1% in 0.9% NaCl, Sigma) was injected through the tail vein. Mice were kept for 1 hr, unless otherwise specified, before sacrificing. Skin samples were dissected, photographed, and either placed in formamide at 56°C for 36 hr to extract Evans Blue or fixed for further immunostaining. Alternatively, dry-ice-frozen samples were saved for western blot analysis, and total proteins were extracted from ~0.2 cm^2 crashed in 50 μl 2× Laemmli buffer. Noninjected skin samples were used to normalize quantification of dye extravasation, read by spectrophotometry at 620 nm.

In Vitro Permeability, Migration, and Proliferation Assays

Permeability assays were conducted as described previously (Gavard and Gutkind, 2006). Briefly, endothelial cells were grown as a 3-day-old mature monolayer on collagen-coated 3 μm-size pore inserts (PTFE, Corning Costar, Acton, MA). Cells were starved overnight, treated as required, and incubated with FITC-dextran (60 kDa, 1 mg/ml, Molecular Probes, Invitrogen). Each sample from the bottom chamber was read in triplicate on the Victor 3V1420 multicounter (Perkin-Elmer, Wellesley, PA). Endothelial migration was assessed by wound-closure assays. Three-day-old endothelial monolayers were starved overnight and wounded by a bevel-edged needle. Wound closures were monitored 18 hr later in serum-free medium or in the presence of VEGF and Ang1. Proliferation was estimated by BrdU incorporation. Three-day-old endothelial monolayers were starved for 24 hr and incubated in serum-free medium with VEGF and Ang1 for an additional 18 hr. BrdU (10 μM, Sigma) was added to the medium 4 hr before fixation. DNA was denaturated by incubation in 0.5% PBS-Triton-2N HCl for 30 min at 37°C, and pH was recovered by sequential washes in 0.1 M borate (pH 8.0) and PBS before staining with rat anti-BrdU monoclonal antibodies (Accurate Chemical and Scientific Corp., Westbury, NY).

Internalization Assays and Immunofluorescence

The internalization assay protocol was described previously by Gavard and Gutkind (2006). Briefly, cells were incubated in DMEM with anti-VE-cadherin (BV6 clone) at 4°C for 1 hr. The antibody uptake was induced for 30 min at 37°C in serum-free medium or in the presence of VEGF and Ang1. Cells were either fixed or subjected to a mild acid wash (2 mM PBS-glycine [pH 2.0], 15 min) in order to remove plasma membrane-bound antibodies. Immunofluorescence staining was done as described in Gavard and Gutkind (2006). Cryostat sections were obtained from fixed, frozen skin samples. Permeabilization was done for 1 hr at room temperature in ICC buffer (0.05% PBS-Tween-3% BSA). Antibody incubations were done for 16 hr at 4°C in ICC buffer, followed by four 15 min washes in the same buffer. Confocal acquisitions were performed on a TCS/SP2 Leica microscope (NIDCR Confocal Facility, NIH, Bethesda, MD).

GST Pull-Downs, Immunoprecipitations, and Western Blots

Rac and RhoA activation was monitored by GST pull-downs by using GST-PAK-CRIB (Cdc42/Rac Interacting Binding domain) and GST-Rhotekin recombinant proteins, respectively, bound to glutathion slurry resin (Amersham Biosciences, General Electrics, Piscataway, NJ). Cells were lysed in Magnesium Buffer (10 mM Tris [pH 7.5], 100 mM NaCl, 1% Triton, 0.5 mM EDTA, 40 mM β-glycerophosphate, 10 mM $MgCl_2$, 1 mM Na_3VO_4, 10 μg/ml aprotinin, 10 μg/ml leupeptin, and 1 mM PMSF), and postnuclei supernatants were incubated for 30 min at 4°C with slurry resin. Immunoprecipitations were performed by using the TNT buffer (10 mM Tris [pH 7.4], 150 mM NaCl, 1% NP40, 1% Triton, 2 mM EDTA and 1 mM Na_3VO_4, 10 μg/ml aprotinin, 10 μg/ml leupeptin, and 1 mM PMSF). For western blot analysis, equal amounts of proteins were separated on 4%–20% polyacrylamide SDS Tris-glycine gels (Invitrogen) and transferred on PVDF membranes (Millipore, Billerica, MA). Horseradish peroxidase activity was revealed by a chemoluminescence reaction (ECL, Pierce, Rockford, IL).

Fluorescence Resonance Energy Transfer Analysis

Src activation was monitored by the use of a genetically encoded fluorescent reporter for Src. This sensor consists of fusions of cyan fluorescent protein (CFP, donor), a phosphotyrosine-binding domain (Src homology domain SH2), a consensus substrate for Src phosphorylation, and yellow fluorescent protein (YFP, acceptor) (Ting et al., 2001). In endothelial cells, stimulation of Src kinase activity causes a 15%–20% increase in the YFP/CFP emission ratio because of phosphorylation-induced conformational changes leading to FRET. Emission spectra and ratios (527 nm/476 nm, YFP/CFP) were measured in 96-well plates at 433 nm excitation on a Tecan Fluorimeter. Normalization was done with respect to the unstimulated transfected cells on both CFP and YFP relative emitted fluorescence units (12 wells for each experiment). Imaging was monitored by using the AxioVert microscope (Zeiss), equipped with a FRET cube filter set from Zeiss and AxioFRET software. FRET analysis and quantification were performed according to the manufacturer's protocols.

Supplemental Data

Supplemental Data include six figures and are available with this article online at http://www.developmentalcell.com/cgi/content/full/14/1/25/DC1/.

ACKNOWLEDGMENTS

This research was supported by the Intramural Research Program of the National Institutes of Health (NIH), National Institute of Dental and Craniofacial Research (NIDCR). We thank C.J. Edgell (UNC, NC), R.Y. Tsien (UCSD, CA), A.S. Alberts (Van Andel Research Institute, MI), and M.K. Rosen (UTSD, TX) for providing reagents, and P. Amornphimoltham (NIH, NIDCR), T. Palmby (NIH, NIDCR), and N. Bidere (NIH, National Institute of Allergy and Infectious Diseases) for comments and discussions. J.G. and J.S.G. planned the experimental design, analyzed data, and wrote the paper, and J.G. and V.P. conducted the experiments. The authors declare that they have no competing financial interests.

Received: July 9, 2007
Revised: October 5, 2007
Accepted: October 31, 2007
Published: January 14, 2008

REFERENCES

Birukova, A.A., Birukov, K.G., Gorshkov, B., Liu, F., Garcia, J.G.N., and Verin, A.D. (2005). MAP kinases in lung endothelial permeability induced by microtubule disassembly. Am. J. Physiol. Lung Cell. Mol. Physiol. *289*, L75–L84.

Burridge, K. (1999). Crosstalk between Rac and Rho. Science *283*, 2028–2029.

Cascone, I., Audero, E., Giraudo, E., Napione, L., Maniero, F., Philips, M.R., Collard, J.G., Serini, G., and Bussolino, F. (2003). Tie-2-dependent activation of RhoA and Rac1 participates in endothelial cell motility triggered by Angiopoietin-1. Blood *102*, 2482–2490.

Chou, M.T., Wang, J., and Fujita, D.J. (2002). Src kinase becomes preferentially associated with the VEGFR, KDR/Flk-1, following VEGF stimulation of vascular endothelial cells. BMC Biochem. *3*, 32.

Copeland, S.J., Green, B.J., Burchat, S., Papalia, G.A., Banner, D., and Copeland, J.W. (2007). The diaphanous inhibitory domain/diaphanous autoregulatory domain interaction is able to mediate heterodimerization between mDia1 and mDia2. J. Biol. Chem. *279*, 30120–30130.

Dumont, D.J., Gradwohl, G., Fong, G.H., Puri, M.C., Gertsenstein, M., Auerbach, A., and Breitman, M.L. (1994). Dominant-negative and targeted null mutations in the endothelial receptor tyrosine kinase, tek, reveal a critical role in vasculogenesis of the embryo. Genes Dev. *8*, 1897–1909.

Edgell, C.J., McDonald, C.C., and Graham, J.B. (1983). Permanent cell line expressing human factor VIII-related antigen established by hybridization. Proc. Natl. Acad. Sci. USA *80*, 3734–3737.

Eliceiri, B.P., Paul, R., Schwartzberg, P.L., Hood, J.D., Leng, J., and Cheresh, D.A. (1999). Selective requirement for Src kinases during VEGF-induced angiogenesis and vascular permeability. Mol. Cell *4*, 915–924.

Ferrara, N., Carver-Moore, K., Chen, H., Dowd, M., Lu, L., O'Shea, K.S., Powell-Braxton, L., Hillan, K.J., and Moore, M.W. (1996). Heterozygous embryonic lethality induced by targeted inactivation of the VEGF gene. Nature *380*, 439–442.

Gamble, J.R., Drew, J., Trezise, L., Underwood, A., Parsons, M., Kasminkas, L., Rudge, J., Yancopoulos, G., and Vadas, M.A. (2000). Angiopoietin-1 is an

antipermeability and anti-Inflammatory agent in vitro and targets cell junctions. Circ. Res. *87*, 603–607.

Garrett, T.A., Van Buul, J.D., and Burridge, K. (2007). VEGF-induced Rac1 activation in endothelial cells is regulated by the guanine nucleotide exchange factor Vav2. Exp. Cell Res. *313*, 3285–3297.

Gavard, J., and Gutkind, J.S. (2006). VEGF controls endothelial-cell permeability by promoting the β-arrestin-dependent endocytosis of VE-cadherin. Nat. Cell Biol. *8*, 1223–1234.

Jho, D., Mehta, D., Ahmmed, G., Gao, X.-P., Tiruppathi, C., Broman, M., and Malik, A.B. (2005). Angiopoietin-1 opposes VEGF-induced increase in endothelial permeability by inhibiting TRPC1-dependent Ca2 influx. Circ. Res. *96*, 1282–1290.

Jones, N., Iljin, K., Dumont, D.J., and Alitalo, K. (2001). Tie receptors: new modulators of angiogenic and lymphangiogenic responses. Nat. Rev. Mol. Cell Biol. *2*, 257–267.

Lampugnani, M.G., Orsenigo, F., Gagliani, M.C., Tacchetti, C., and Dejana, E. (2006). Vascular endothelial cadherin controls VEGFR-2 internalization and signaling from intracellular compartments. J. Cell Biol. *174*, 593–604.

Lee, S., Chen, T.T., Barber, C.L., Jordan, M.C., Murdock, J., Desai, S., Ferrara, N., Nagy, A., Roos, K.P., and Iruela-Arispe, M.L. (2007). Autocrine VEGF signaling is required for vascular homeostasis. Cell *130*, 691–703.

Li, X., Hahn, C.N., Parsons, M., Drew, J., Vadas, M.A., and Gamble, J.R. (2004). Role of protein kinase Cζ in thrombin-induced endothelial permeability changes: inhibition by Angiopoietin-1. Blood *104*, 1716–1724.

Mammoto, T., Parikh, S.M., Mammoto, A., Gallagher, D., Chan, B., Mostoslavsky, G., Ingber, D.E., and Sukhatme, V.P. (2007). Angiopoietin-1 requires p190RhoGAP to protect against vascular leakage in vivo. J. Biol. Chem. *282*, 23910–23918.

Marinissen, M.J., Chiariello, M., Tanos, T., Bernard, O., Narumiya, S., and Gutkind, J.S. (2004). The small GTP-binding protein RhoA regulates c-jun by a ROCK-JNK signaling axis. Mol. Cell *14*, 29–41.

Palazzo, A.F., Cook, T.A., Alberts, A.S., and Gundersen, G.G. (2001). mDia mediates Rho-regulated formation and orientation of stable microtubules. Nat. Cell Biol. *3*, 723–729.

Pizurki, L., Zhou, Z., Glynos, K., Roussos, C., and Papapetropoulos, A. (2003). Angiopoietin-1 inhibits endothelial permeability, neutrophil adherence and IL-8 production. Br. J. Pharmacol. *139*, 329–336.

Potter, M.D., Barbero, S., and Cheresh, D.A. (2005). Tyrosine phosphorylation of VE-cadherin prevents binding of p120- and {β}-catenin and maintains the cellular mesenchymal state. J. Biol. Chem. *280*, 31906–31912.

Senger, D.R., Galli, S.J., Dvorak, A.M., Perruzzi, C.A., Harvey, V.S., and Dvorak, H.F. (1983). Tumor cells secrete a vascular permeability factor that promotes accumulation of ascites fluid. Science *219*, 983–985.

Seth, A., Otomo, C., and Rosen, M.K. (2006). Autoinhibition regulates cellular localization and actin assembly activity of the diaphanous-related formins FRL{α} and mDia1. J. Cell Biol. *174*, 701–713.

Stockton, R.A., Schaefer, E., and Schwartz, M.A. (2004). p21-activated kinase regulates endothelial permeability through modulation of contractility. J. Biol. Chem. *279*, 46621–46630.

Suri, C., Jones, P.F., Patan, S., Bartunkova, S., Maisonpierre, P.C., Davis, S., Sato, T.N., and Yancopoulos, G.D. (1996). Requisite role of Angiopoietin-1, a ligand for the TIE2 receptor, during embryonic angiogenesis. Cell *87*, 1171–1180.

Suri, C., McClain, J., Thurston, G., McDonald, D.M., Zhou, H., Oldmixon, E.H., Sato, T.N., and Yancopoulos, G.D. (1998). Increased vascularization in mice overexpressing Angiopoietin-1. Science *282*, 468–471.

Thurston, G., Suri, C., Smith, K., McClain, J., Sato, T.N., Yancopoulos, G.D., and McDonald, D.M. (1999). Leakage-resistant blood vessels in mice transgenically overexpressing Angiopoietin-1. Science *286*, 2511–2514.

Thurston, G., Rudge, J.S., Ioffe, E., Zhou, H., Ross, L., Croll, S.D., Glazer, N., Holash, J., McDonald, D.M., and Yancopoulos, G.D. (2000). Angiopoietin-1 protects the adult vasculature against plasma leakage. Nat. Med. *6*, 460–463.

Ting, A.Y., Kain, K.H., Klemke, R.L., and Tsien, R.Y. (2001). Genetically encoded fluorescent reporters of protein tyrosine kinase activities in living cells. Proc. Natl. Acad. Sci. USA *98*, 15003–15008.

Tominaga, T., Sahai, E., Chardin, P., McCormick, F., Courtneidge, S.A., and Alberts, A.S. (2000). Diaphanous-related formins bridge Rho GTPase and Src tyrosine kinase signaling. Mol. Cell *5*, 13–25.

Uemura, A., Ogawa, M., Hirashima, M., Fujiwara, T., Koyama, S., Takagi, H., Honda, Y., Wiegand, S.J., Yancopoulos, G.D., and Nishikawa, S. (2002). Recombinant Angiopoietin-1 restores higher-order architecture of growing blood vessels in mice in the absence of mural cells. J. Clin. Invest. *110*, 1619–1628.

Wallar, B.J., and Alberts, A.S. (2003). The formins: active scaffolds that remodel the cytoskeleton. Trends Cell Biol. *13*, 435–446.

Weis, S., Shintani, S., Weber, A., Kirchmair, R., Wood, M., Cravens, A., McSharry, H., Iwakura, A., Yoon, Y.S., Himes, N., et al. (2004). Src blockade stabilizes a Flk/cadherin complex, reducing edema and tissue injury following myocardial infarction. J. Clin. Invest. *113*, 885–894.

Wojciak-Stothard, B., and Ridley, A.J. (2002). Rho GTPases and the regulation of endothelial permeability. Vascul. Pharmacol. *39*, 187–199.